

DIRECTIONAL ANTENNAS FOR COGNITIVE RADIO: ANALYSIS AND DESIGN RECOMMENDATIONS

Noman Murtaza*, Rajesh K. Sharma, Reiner S. Thomä, and
Matthias A. Hein

Institute for Information Technology, Ilmenau University of Technol-
ogy, Ilmenau 98693, Germany

Abstract—Cognitive radio technology proposes the utilisation of under-utilised spectrum resources which may include time, frequency, geographical location, direction, polarisation et cetera. Frequency is the conventional spectrum resource, considered to be exploited for cognitive radio, especially in the field of antenna design. We address the unconventional directional resource for cognitive radio, from antenna design perspective. The design concept of a multi-band compact array, capable of providing separate and simultaneous access to frequency and directional resources, is presented. The initial explorations are carried out for three frequency resources (bands) and three directional resources, providing nine degrees-of-freedom altogether. Laboratory version of the proposed antenna system is then used to gain proof-of-principle through line-of-sight measurements in an over-the-air test-bed, followed by static outdoor measurements in a multipath scenario. At the end, simulations are performed for arbitrary arrays in heterogeneous propagation scenarios to study the influence of antenna radiation pattern on the availability of directional opportunity. Recommendations are made for possible antenna design based on the simulation results.

1. INTRODUCTION

The allocation of frequency spectrum to licensed users gives rise to spectrum scarcity, considering the increasing demands of capacity in the existing and emerging communication standards. Occupancy of the allocated spectrum by licensed users, referred to as primary users (PU) in cognitive radio (CR) community, varies over time and geographical

Received 11 March 2013, Accepted 13 May 2013, Scheduled 22 May 2013

* Corresponding author: Noman Murtaza (noman.murtaza@tu-ilmenau.de).

location. This fact has been investigated through various measurement campaigns, for example, [1, 2]. Such a spectrum underutilisation provides an opportunity for secondary users (SU) to use the licensed spectrum through CR technology [3, 4]. It should, however, be ensured that PU is not interfered.

Hence, the spectrum occupancy of PU must be continuously monitored such that the white spaces are detected for SU communication and the spectrum is released as soon as PU reappears. PU activities can be monitored using various sensing algorithms, for example, energy detection [6], matched filtering, feature detection [7], correlation-based detection [5] et cetera. *Energy detection* is used for the analyses in this paper because of its simplicity and no need of a-priori information. Nevertheless, we expect that the choice of sensing algorithm would have little influence on the conclusions drawn in this paper.

Frequency resource has been extensively studied for CR, especially in the context of antenna design. Various CR system architectures discussed in [8], identify the possibilities for antenna design. These include two separate antennas for sensing and transmission, a single wide band antenna, and a reconfigurable narrowband antenna. The focus of antenna design for CR has remained on a two-antenna approach for a long time. Such antenna designs consisted of a wideband antenna for sensing and a reconfigurable narrowband antenna for CR communication. In this respect, [9] presented a two-port antenna for cognitive radio where communication antenna was made multi-band using defected ground plane, [11] employed switches along the length of a microstrip monopole to define resonance frequencies for communication antenna, [10] proposed a rotatable two-port antenna where the resonance frequency of the communication antenna was changed by rotating a set of antenna structures. It is important to notice that such antennas provide only a few reconfigurable communication states.

Recently, single-port antenna designs have been proposed that consist of a wideband antenna with reconfigurable filters to provide access to a few narrow frequency bands [12] for overlay CR communications, and to reject narrow frequency bands [13] for underlay CR communications. Such an arrangement of filters on the radiating aperture of the antenna is likely to disturb the aperture field distribution and hence the radiation properties of the antenna.

However, frequency resource alone may not be sufficient to fulfil the needs of future communication systems. Future spectrum access technologies could imagine cognition beyond mere frequency resource [14]. A combination of frequency, space/direction and time

can ensure a more efficient use of spectrum by employing techniques like direction-of-arrival estimation, interference mitigation et cetera. For example, making use of multiple antennas in the form of antenna arrays enables direction sensing and hence in location awareness of primary users which can subsequently help in avoiding interference to PU, using (digital) beamforming while exploiting occupied licensed channels. The utilisation of directional patterns for transmission and reception can, in addition, increase the link budget of a communication system by increasing directivity in certain directions and reducing interference from others. Hence, situations like heterogeneous path loss conditions between primary and secondary systems [15], relay-assisted transmission of secondary users [16] et cetera may allow directional re-use of frequency spectrum.

Multiple receive antennas have been used for CR for primary user detection [15, 16] and/or interference suppression [17]. Pattern reconfigurable antennas have also been proposed in literature. For example, [18] suggests an antenna that selects frequency and pattern by choosing one or multiple dipoles, [19] suggests an optoelectronic switch which could be used for frequency selectivity and pattern adaptability, [20] uses PIN diodes on annular slot antenna for null-steering.

We propose a novel antenna design concept enabling frequency- and direction-selective sensing and communication. Such an antenna system employs multi-band compact antenna arrays together with a (reconfigurable) feed network allowing access to each degree-of-freedom *simultaneously and separately* at port level. The reconfigurability of the proposed antenna system is located in the feed network, where detrimental effects on the radiation pattern are minimised. Different patterns can be selected by addressing different input ports of the feed network, opening up the potential of full reconfigurability through digital beamforming. The design of the proposed feed network is left out of scope for this paper. The pattern selectivity is, however, achieved using absorber/metal walls for proof-of-principle measurements.

The analysis of directional antennas for CR can be carried out through measurements, modelling, and/or emulation. The Measurement campaigns may be performed outdoor or inside an anechoic chamber. Over-the-air (OTA) measurements inside an anechoic chamber provide the flexibility to test the performance of the antenna in a controlled environment [21, 26]. This helps in recognising the limitations of the whole RF chain including the antenna systems in real environment. The proposed antenna system was first characterised in a line of sight OTA scenario. As the results indicated a reasonable signal to interference ratio, outdoor measurements were performed.

The analysis was continued with spatial channel model to determine the performance of antenna arrays with fixed directional patterns in heterogeneous propagation scenarios.

Design considerations for directional antennas with spectral and directional access for CR are discussed in Section 2. Proof-of-principle measurement campaigns with the laboratory versions of the proposed antenna system are presented in Section 3. The simulation results for heterogeneous propagation scenarios, in the context of optimum antenna design for CR communications are discussed in Section 4. The paper concludes with a brief discussion.

2. DESIGN CONSIDERATIONS FOR DIRECTIONAL ANTENNAS FOR COGNITIVE RADIO

2.1. Spectral and Spatial Bins

The antenna for cognitive radio may not provide access to infinite frequency resources and yet be highly adaptable in terms of its spatial selectivity. Hence, a choice has to be made on the frequency bands of interest and spatial adaptability.

The focus of our work is on the use of CR in disaster scenarios where the infrastructure is expected to be damaged and several users are pending to service. While the repair of the infrastructure may take days and weeks, CR that is adaptable to the environment can be utilised immediately to establish missing links. Hence, we are specifically interested in the existing infrastructure, for example, GSM1800, GSM900, and IEEE 802.11b/g as the frequency resources. For initial study, we restrict ourselves to three directional resources, covering 360° in azimuth, at all frequency resources.

2.2. Spectral and Spatial Interface

An ideal antenna for spectral and spatial sensing should be multi-band, able to detect the spectral resources in different directions using multiple beams. The antenna designs described in literature so far provide all communication degrees-of-freedom to be accessible at one port, through a few reconfigurable states. The resources are therefore separable only through analogue or digital signal processing after the antenna port. Moreover, the current designs consider filters to be directly embedded into the antenna which may also deteriorate the radiative properties and efficiency of the antenna. We want to define this interface more carefully. Hence we propose to add spatial and spectral interfaces disembodied from the actual antenna. This would ensure undisturbed radiative properties of the antenna.

We propose to use compact multi-band antenna arrays with a carefully designed feed network as a solution to access all the spatial and spectral degrees-of-freedom simultaneously yet separably, by providing a separate port for each degree-of-freedom. Compared to conventional antenna designs for cognitive radio, such an antenna system would provide additional access to the *unconventional* directional resource, the importance of which is highlighted through the following simulation and measurement campaigns. However, since the design of such an antenna system involves antenna arrays, the physical size is bigger compared with conventional frequency reconfigurable antennas discussed in literature. However physical as well as electrical sizes are proposed to be reduced using compact arrays with reduced element spacing. We present only the first proof-of-principle design approach, with no specific application in mind, and correspondingly no efforts for ultimate miniaturisation. The size can be further reduced by an appropriate choice of the individual antenna element (monopole, slot, patch et cetera) and array arrangement.

The sensing strategy in mind is that the antenna searches for all degrees-of-freedom in the sensing mode and then utilises the best available opportunity by connecting to the respective degree-of-freedom in the communication mode. If a separate communication transceiver is available, the antenna can sense and transmit at the same time. With a careful design of the waveform, it may be possible to access multiple degrees-of-freedom at the same time to enhance the capacity of the secondary link.

2.3. Flexibility versus Complexity

A fully adaptive array with highly controllable radiation pattern (beamwidth, side-lobe level et cetera) would require a large number of elements with a tunable phase-shifter and a tunable amplifier behind every element, resulting in a complex antenna system with high power consumption.

We propose an antenna system, consisting of a multi-band multi-port array and a multi-band multi-port feed network, that provides the spectral and spatial selectivity at the system port level. In its full capability, the CR node can process each degree-of-freedom simultaneously. This would, however, lead to a complex, expensive and power-consuming hardware. On the other extreme, switching circuits can be used to access the degrees-of-freedom in a consecutive way (time division multiplexing). This would, however, introduce latency depending on the switching speed. This trade-off exists and is not studied within the scope of this paper.

The complexity of such an antenna system would also increase

with an increase of the degrees-of-freedom. An increase of the *directional* degrees-of-freedom would introduce complexity in the feed network and an increase of the *frequency* degrees-of-freedom would require extra feed networks. Hence, flexibility can be introduced at the expense of complexity. For the initial explorations, we limited ourselves to three frequencies and three directions, giving rise to nine degrees-of-freedom in total. We consider such an approach sufficient for evaluation and discussion, as well as realistic for the applications we have in mind.

2.4. Proposed Antenna Design

In order to design an elementary antenna system with individual access to frequency degrees-of-freedom, we propose concentric antenna arrays resonant at three selectable frequency bands: GSM900, GSM1800, and IEEE 802.11b/g. The frequencies are visualised with nine $\lambda/4$ -monopoles over ground. Three of these nine monopoles (resonant at one frequency) are placed at vertices of an equilateral triangle. These triangles of monopoles form an array at 900 MHz (outer), 1800 MHz (middle) and 2450 MHz (inner) as shown in Figure 1. The directional selectivity in this antenna may be achieved with the help of a multi-band feed network behind the antenna array as shown in Figure 2. Moreover, such an arrangement can be made compact by reducing the electrical spacing between the array elements. Such a compact multi-band multi-port antenna array must, therefore, be connected to a multi-band decoupling and matching network while preserving

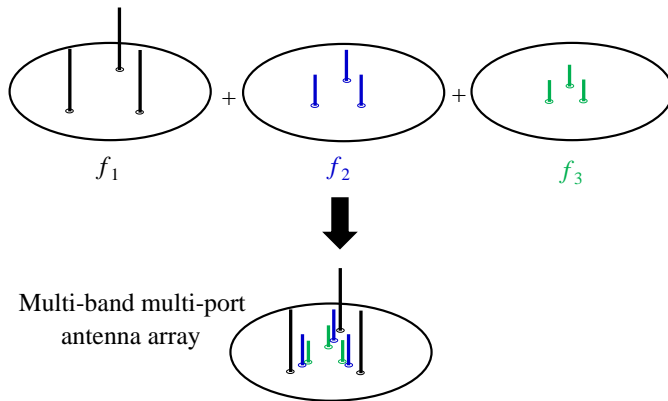


Figure 1. Sketch and formation of the proposed generic multi-band multi-port antenna array operating at three frequencies f_1 , f_2 , and f_3 (different colours).

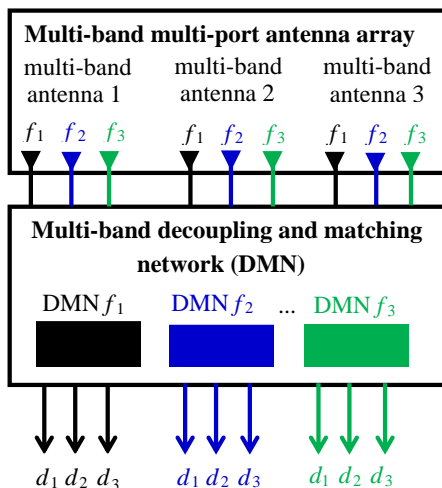


Figure 2. Generic block diagram of the multi-band directional antenna system consisting of a multi-band multi-port antenna array and a multi-band feed network (decoupling and matching network in case of compact arrays). Such an antenna system provides simultaneous and separate access to frequency (frequencies f_1 , f_2 , and f_3) and spatial degrees-of-freedom (directions d_1 , d_2 , and d_3).

the port-level access to all degrees-of-freedom. This multi-band feed network can be combined into one network using reconfigurable components, for example, varactor diodes as discussed in [22] or switching between individual network elements as discussed in [23]. Moreover, the individual feed networks can also be made reconfigurable to cover a range of frequencies within a certain band of interest. The tuning ranges may vary from a few hundred MHz to 1 GHz depending on the number of tunable components in the network. Such a reconfigurability behind the antenna aperture does not influence the radiation properties of the antennas as in case of the state-of-art reconfigurable antennas. The design of the feed network for such an antenna array is out of scope for this paper. We rather focus on the feasibility of such an array arrangement for identification of directional opportunities through measurements and simulations. Measurements were performed to evaluate the capability of the proposed antenna system, and to identify the existence of directional resources for CR. The simulations were then performed to extend the results achieved from measurements and make recommendations for suitable directional antenna design for CR communication.

3. PROOF-OF-PRINCIPLE MEASUREMENT CAMPAIGNS

Measurements were performed for a line-of-sight (LOS) and a multipath scenario using laboratory versions of the proposed antenna systems with an inter-element spacing of $\lambda/2$. The LOS measurements were performed in an anechoic chamber while the multipath measurement campaign was performed outdoor.

3.1. Line-of-sight Measurements in an over-the-air Test Setup

A laboratory version of the CR node was tested in receive mode in an over-the-air (OTA) test setup. The detailed measurement campaign was reported in [24]. A brief insight into the campaign is provided in the following.

3.1.1. CR Node

The CR node consisted of a multi-band directional antenna connected to a commercial wideband transceiver USRP2 (universal software radio peripheral) from Ettus research lab [25], which was accessed with MATLAB for reconfiguration and baseband processing. These two building blocks form a CR node that is used for sensing. The directional antenna consisted of a square, instead of a circular, ground in this experiment as shown in Figure 3(a). The comparative study of circular and square ground plane did not reveal significant differences in terms of the feasibility of the idea. The directional patterns, in this basic experiment, were obtained by placing a Y-shaped absorber walls between the elements of the proposed antenna array. The absorber walls divide the hemisphere above ground plane in three distinct sectors (135° , 90° and 135°) as shown by the resulting measured radiation patterns in Figure 3(b). The radiation patterns in different directions are not identical because of asymmetric ground conditions in different sectors. This asymmetry in the radiation patterns does not influence the following analysis.

A switch network was used behind the antenna arrangement to provide separate and consecutive access to all degrees-of-freedom using a single wideband receiver. The initialization and control of the USRP2 devices, data acquisition, switch control, and post-processing was implemented in MATLAB on a personal computer. USRP2 was used for off-line instead of real-time processing. We used *RFX2400* (full-duplex transceiver for Wi-Fi frequency range of 2.3–2.9 GHz) and *WBX* (full-duplex wideband transceiver for 50 MHz–2.2 GHz)

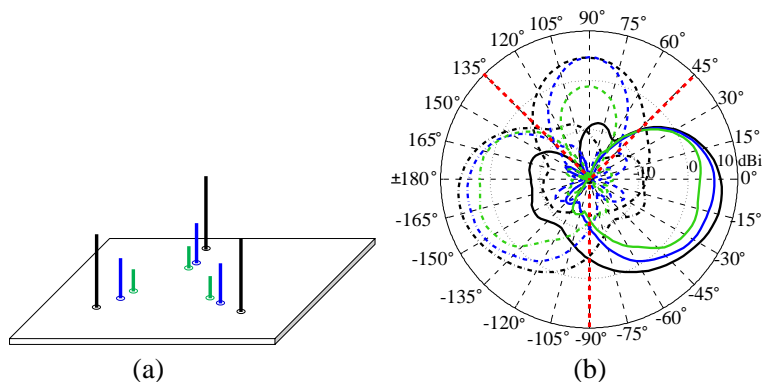


Figure 3. The antennas operating at 900 MHz, 1800 MHz, and 2450 MHz and their respective radiation patterns are shown in black, blue, and green colour respectively. 18 cm tall absorber walls were used in this design to define directional patterns d_1 (solid), d_2 (dashed), and d_3 (dotted). The placement of absorber walls are shown by dashed red lines. The ground plane measures 40 cm \times 40 cm. (a) Sketch of the multi-band multi-port antenna array used for line-of-sight measurements. (b) θ -cut of the antenna system with square ground plane and Y-shaped absorber walls.

daughter boards for the realization of the CR node. Averaging over 100 samples per snapshot was used for elimination of time variant non-idealities of the receiver. For the observation of frequency ranges wider than the transfer bandwidth of 25 MHz, the carrier frequency was swept.

3.1.2. OTA Test Setup

Over-the-air testing accounts for real antenna and radio channel characteristics and enables the simultaneous excitation of the CR node from different directions at different frequencies. For an initial measurement, we used a static channel without any distinction between primary and secondary users, thereby emulating line-of-sight (LOS) links between the cognitive node and virtual surrounding users. The CR node was not used for uplink within this measurement campaign. The details of the OTA testbed for CR nodes were discussed in [21]. This test was the first phase of a projected more complex OTA test and deals with an observation of radio environment under LOS conditions only.

Eight wideband transmit antennas were used in a circular

arrangement. The antennas were mounted on a wooden structure, as illustrated by Figure 4. The transmit antennas consisted of six Vivaldi antennas with a gain varying between 2 and 7 dBi across a frequency range from 1.8 to 3 GHz, and two log-periodic dipole antennas (LP0926 by Ettus [25]) with a gain of 5 to 6 dBi in the range of 900–2600 MHz. Each transmit antenna was fed with a fictitious user signal. Two of these signals were transmitted in the 900 MHz band, three in the 1800 MHz band, and three in the 2450 MHz band.

A static 9 MHz wide multi-carrier signal, generated by a vector signal generator (R&S SMU200A), was used as the main test signal [24]. This test signal was up-converted to the aforementioned frequency bands with the help of mixers of a wideband fading emulator (Elektrobit PROPSim C8). Since the measurements were LOS, the full capability of the fading emulator was not used. Arbitrary waveform/vector signal generators by R&S and Agilent were used as local oscillators. As a consequence of mixing of the channel emulator, only the lower side-band could be used. Figure 5 shows a picture of the whole signal generation setup in the control room of the anechoic chamber. An illustration of the different test signals (power spectra) and an allocation to the transmit antennas is provided by Figure 6. The power level of the main transmit signal was -5 dBm. Each local oscillator (LO) had a power of 0 dBm. To cope with the cable attenuation (about 5 to 6 dB), we used a bank of power amplifiers

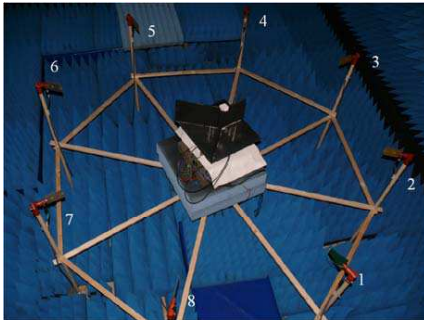


Figure 4. The CR node (antenna arrays with absorber walls, USRP2 and switch network) placed in the centre of OTA ring. The antennas #1–#8 denote the illuminating antennas of the OTA ring [24].



Figure 5. OTA signal generation setup with the different measurement units indicated in the figure and further explained in the main text [24].

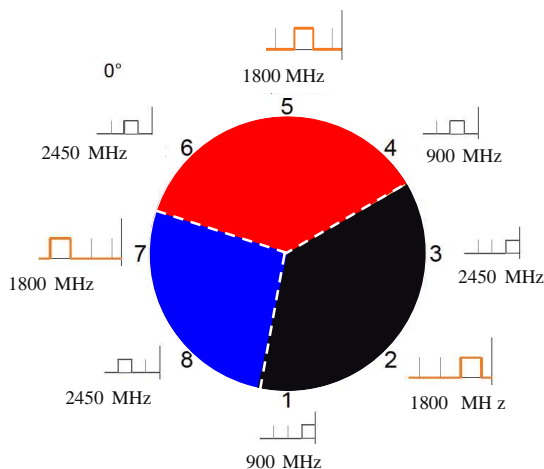


Figure 6. Illustration of the OTA test signals (power spectra histograms along the outer contour of the diagram). There were only two 900 MHz signals (terminals #1 and #4). Starting from the reference point (terminal #8, in the 0° direction), the antenna with the three segments (blue, red, black) was rotated counter-clockwise.

(PAs, Mini-circuits ZX60-2534M+).

At the beginning of the OTA test, we checked the setup in a conducted way, to calibrate attenuations and emulator settings. Next, we calibrated the signals for OTA transmission to have a magnitude of -15 dBm at the output of the PAs. Thereafter, we performed the actual OTA-test by rotating the receiver antenna system of the CR node in steps of 45° .

3.1.3. Measurement Results and Discussion

Each measurement at the different frequencies and directions revealed the desired signal, the interference from other directions, and further non-idealities from the receiver. The power spectral density (PSD) sensed from different directions is shown in Figure 7 at 1800 MHz as an example. In general, we could recognize a signal-to-interference (S/I) ratio of 20 dB or more in all frequency bands studied. Figure 7 illustrates the results at 0° orientation of the receive antenna. Similar results were obtained as the antenna was rotated counter clockwise in steps of 45° . However, the interference from undesired directions was at a level of 5 to 10 dB when the transmit terminals were at the border of the dividing absorber walls of the receive antenna (overlap regions

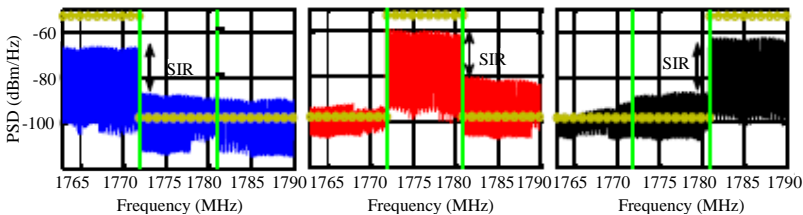


Figure 7. Typical measurement results at 0° (referred to Figure 6) for all receive directions d_1 – d_3 at 1800 MHz. The different coloured signals correspond to the respective sectors in Figure 6. The yellow envelope indicates the expected signals and the green lines separate the signals transmitted in different sectors.

of the respective radiation patterns).

This test yielded a proof-of-principle that if the proposed antenna system provided directional beams with reasonably low side-lobe levels, a good signal to interference and noise ratio (SINR) could be achieved, at least under LOS conditions. The side-lobe level of the directional patterns plays an important role in identification of directional opportunities as discussed further in Section 4.

3.2. Outdoor Measurement Campaign

After the initial LOS measurements, it was reasonable to perform outdoor measurements to observe the situation of directional opportunity in a multipath scenario. The downlink frequency spectrum of the mobile communications operator *Vodafone D2* [27] ranging from 1847.9 MHz to 1852.9 MHz was observed in the outdoor measurements. These measurements were limited to GSM1800, as the objective was to gain a proof-of-principle. The results of this campaign can be generalised for other frequency bands of interest in similar scenarios.

3.2.1. Measurement Setup

The measurement setup consisted of three synchronised wideband receivers (USRP2), a custom-made sector antenna, and a personal computer, as shown in Figure 8. In this measurement campaign, the multi-band monopole array was built on a circular ground plane. This allowed the homogeneous distribution of sectors into 120° each, by placing metal walls between the antenna elements of the multi-band array. The metal walls were used in this design for mechanical strength while obtaining well shaped patterns with low sidelobe level as shown in Figure 9. The metal walls divide the space around the antenna array

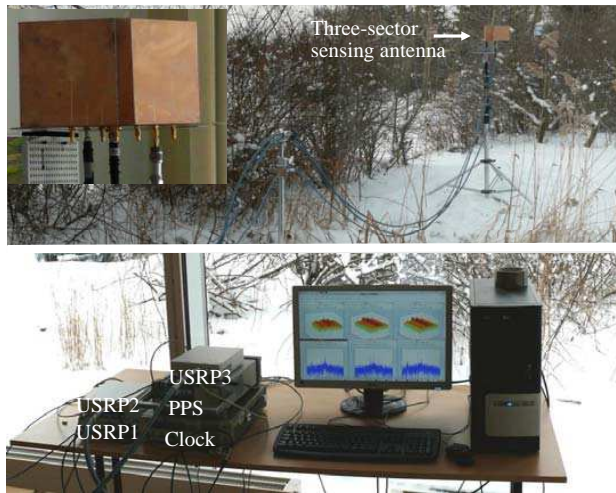


Figure 8. Measurement setup consisting of three synchronised USRPs connected to a three-sector antenna and a personal computer. The clock and pulse per second (PPS) signals were used to synchronise USRPs externally.

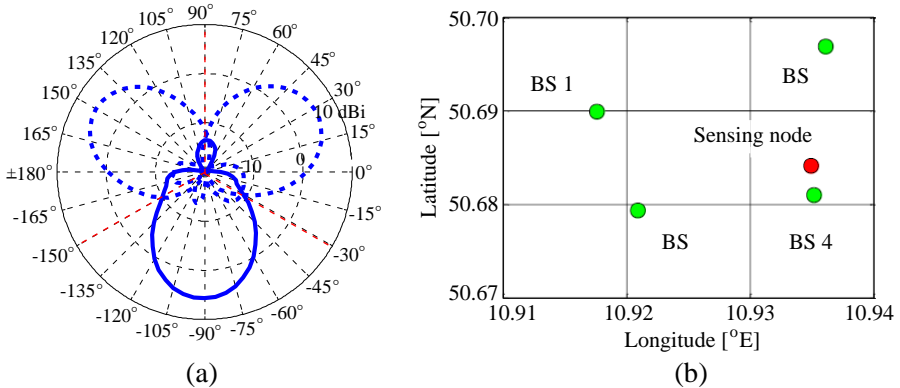


Figure 9. (a) Measured directional patterns d_1 , d_2 , and d_3 of sectors 1, 2, and 3 of the sector antenna with Y-shaped metal walls. The placement of metal walls is shown by dashed red lines. (b) GPS coordinates of base-stations (BS) and sensing node.

into three equal sectors, providing a gain of 5.9 dBi for each sector at the frequency of interest. The sensing node was placed such that each of the directional patterns d_i , $i = 1, 2, 3$ faced a base-station.

The measurements were performed with a data acquisition rate of 2 snapshots/min. The acquired data were saved on a computer and processed off-line using MATLAB.

3.2.2. Analysis

The activity of the primary users in terms of their frequency occupation has been extensively studied in literature, also through measurement campaigns, for example, in [2]. The analysis of this measurement campaign is different in the sense that we want to investigate the directional resources in addition to the frequency resources. We propose to determine the *opportunity* available in different directions, and to analyse the *dissimilarity* of the spectrum occupation among them.

In this measurement campaign, the threshold was chosen to be 23 dB below the global maximum over all snapshots. The binary *opportunity* was calculated on each of the 200 kHz GSM channels within the 5 MHz downlink frequency band (25 GSM channels) of *Vodafone D2*. The received signal strength indicator (*RSSI*) for every GSM channel (CH_{RSSI}) was computed by integrating the power spectral densities. CH_{RSSI} was then compared with the threshold to determine the presence (1) or absence (0) of a secondary communication opportunity. The binary opportunity value was stored in a vector which was then used to compute dissimilar directional opportunities. The choice of the threshold was crucial in this case, as it may over- or under-estimate the opportunity. Depending on the signal-to-noise ratio (SNR), the receiver noise level may already be sufficient to provide a directional opportunity. However, for higher SNR, the threshold must be specified higher than the system noise level depending on the side-lobe level of the directional patterns, their beamwidth and mutual orthogonality.

The dissimilar directional opportunity, defined according to Figure 10, involves the calculation of the *frequency opportunity* for every directional resource. An opportunity is said to be purely *frequency opportunity* (\mathbf{D}_c) if it is available in all directions. A unique *directional opportunity* (\mathbf{D}_u) is present if it is available only in a single direction. This feature can be determined by the logical *XOR* operation among the directional opportunity vectors. Furthermore, the arithmetic mean of \mathbf{D}_c and \mathbf{D}_u can provide the similarity and dissimilarity values respectively. These values can also be expressed as percentage.

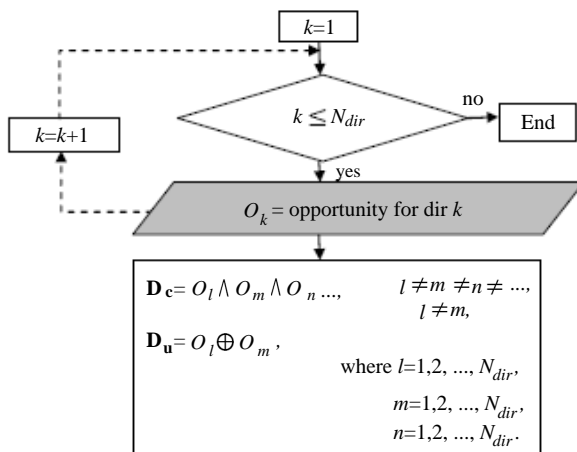


Figure 10. Flow chart describing the dissimilar directional opportunity analysis, the opportunity for all directions is calculated and then compared with others to obtain the common (\mathbf{D}_c) and unique (\mathbf{D}_u) opportunities. \oplus and \wedge represent logical *XOR* and *AND* respectively.

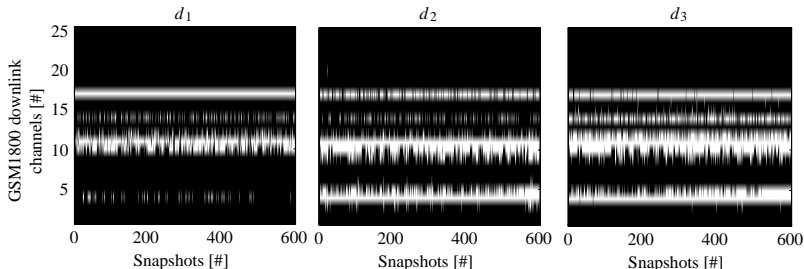


Figure 11. Image plots showing the decision about the occupancy of the *Vodafone D2* GSM1800 downlink channels in different directions d_1 , d_2 , and d_3 in an outdoor environment. The decision threshold is 23 dB below the maximum over all directions and snapshots. Black colour indicates free channels and white colour indicates occupied channels.

3.2.3. Measurement Results and Discussion

The measurement was carried out for five hours giving a total of 600 snapshots. Figure 11 shows the channel occupancy of the *Vodafone D2* downlink frequency band for a decision threshold set 23 dB below the

maximum over all directions and snapshots. For a lower threshold level, the percentage dissimilarity among sectors decreases dramatically. It can be easily seen in Figure 11 that out of 25 available channels, only few (white colour) were used in the cell where the measurements were performed. It is seen that for channel 5 and channel 9, the two directions called d_2 and d_3 show some activity while d_1 is completely free, identifying a unique *directional opportunity*. Channel 4 is sparsely occupied in d_1 while it is highly occupied in d_2 and d_3 . Channels 12 and 14 show high occupancy in d_3 while they are partially free in d_1 and d_2 . Figure 12 shows the opportunity for all three sectors, and the dissimilar directional opportunity between pairs $d_1 - d_2$, $d_1 - d_3$, and $d_2 - d_3$. It can be seen in this figure that although many opportunities are available for channel 9 in all three directions (100%, 67%, and 81%), little dissimilarity (32%, 18%, and 22%) exists among directions. However, channel 4 shows a *directional opportunity* in direction d_1 which is dissimilar to d_2 and d_3 . The remaining channels may be interpreted accordingly.

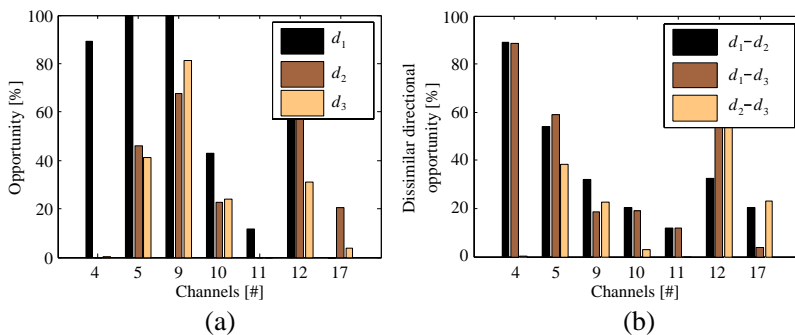


Figure 12. Opportunity seen by (a) sector antenna and (b) dissimilar directional opportunity among directions d_1 , d_2 , and d_3 .

Moreover, the comparison of the dissimilarity among sectors of a directional antenna and an omnidirectional antenna is shown in Figure 13 and Figure 14. This measurement was carried out for two hours, where an omni-directional monopole antenna and two sectors of the sector antenna were connected to the three receivers (because of the limitation on the number of synchronised receivers). Figure 13 and Figure 14 show the channel occupancy, opportunity and dissimilarity detected by the two different antennas. It is worth mentioning that a different frequency spectrum occupancy trend is seen in Figure 13 compared to Figure 11 because the measurements were taken at different times of the day. It can be seen in Figure 13 that

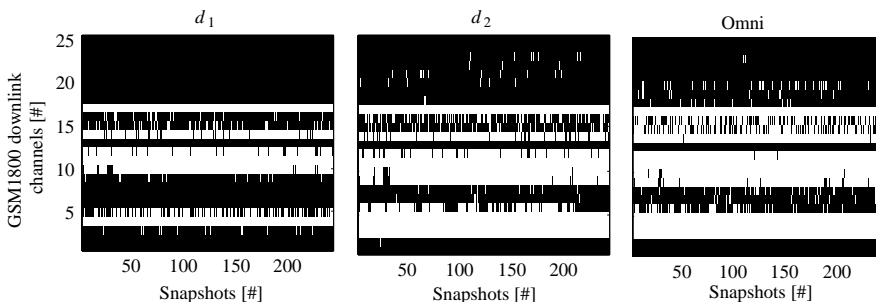


Figure 13. Image plots showing the decision about the occupancy of the *Vodafone D2* GSM1800 downlink channels in directions d_1 , d_2 of the sector antenna, and the omni-directional antenna. The decision threshold is 25 dB below the maximum over all directions and snapshots. Black color indicates free channels and white color indicates occupied channels throughout the paper.

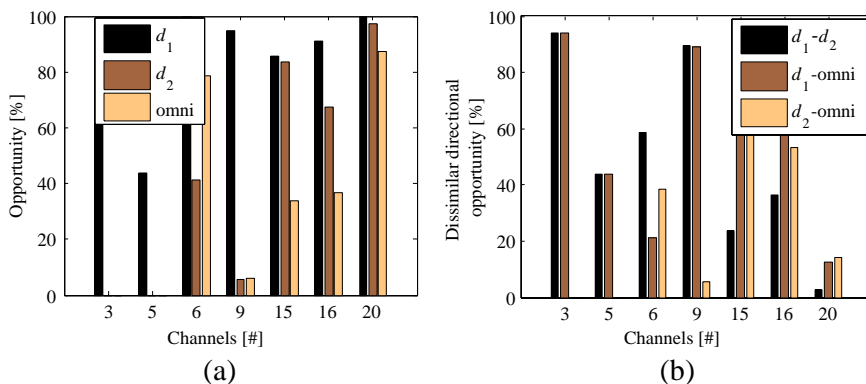


Figure 14. Opportunity seen by d_1 , d_2 of the sector antenna, and (a) the omnidirectional antenna, and (b) the dissimilar directional opportunity among pairs.

the direction d_1 detects many directional opportunities compared with the omni-directional antenna, whereas direction d_2 detects most of the opportunities seen by the omni-directional antenna. The dissimilarity analysis in Figure 14 confirms this result.

The measurement campaigns provide a proof-of-principle that a three-sector antenna can identify directional opportunities for a static CR communication scenario. Furthermore, the proposed directional opportunity analysis was helpful in classification of *frequency* and

directional opportunities. As seen in the results in Figure 12 and Figure 14, looking at the opportunity in different directions separately may be deceiving and result in over-estimation for an omnidirectional opportunity. Comparison of these opportunities is, therefore, crucial in proper identification of directional opportunity.

Nevertheless, measurements were performed for a static scenario and may not be representative for all possible scenarios for CR communication. Hence, a rigorous simulation analysis is performed in Section 4 for heterogeneous propagation scenarios.

4. ANALYSIS OF DIRECTIONAL ANTENNAS IN HETEROGENEOUS PROPAGATION SCENARIOS

Simulations were performed to analyse the influence of the channel properties (propagation scenarios) on directional opportunities, and to investigate the effect of various array patterns on directional opportunity.

4.1. Simulation Framework

A generic block diagram of a CR communication scenario is shown in Figure 15, where a PU transmitter is connected to a CR node through a spatial channel. The simulation framework, therefore, required a spatial channel model, a directional antenna system and directional opportunity analysis at the CR node.

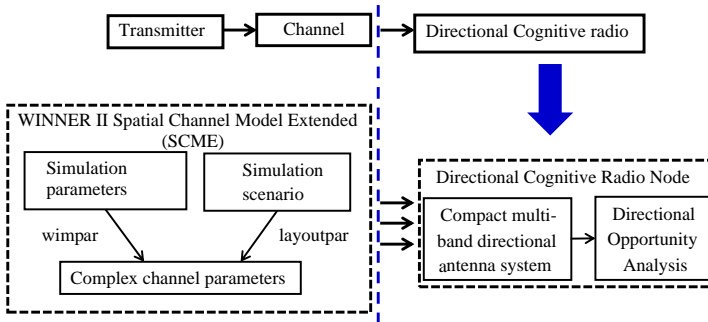


Figure 15. PU transmitter is connected to CR node through a spatial channel. The spatial channel parameters are obtained from WINNER II SCME for simulations. The dashed blue line indicates the interface between the spatial channel and CR node. Details are discussed in the text.

4.1.1. Spatial Channel Model

For preliminary simulations, we used the open-source Winner II Spatial Channel Model Extended (SCME) [28] as the channel between PU and CR node. WINNER II channel model follows a geometry-based stochastic channel modelling approach, which allows creation of an arbitrary radio channel. The channel parameters are determined stochastically, based on statistical distributions extracted from channel measurements. Moreover, the channel models are antenna independent, that is, different antenna configurations and different element patterns can be inserted [28].

To extract the channel parameters from WINNER II channel model, the simulation parameters (e.g., frequency, time samples et cetera) are set in the structure *wimpar*, and the simulation layout (e.g., location of nodes, scenario definition et cetera) is set in the structure *layoutpar*. The model then computes the channel parameters which can be used to embed the antenna characteristics and to perform further signal processing. We used the complex power angular profiles to embed the complex azimuth patterns from measured and analytical antenna arrays. Due to the stochastic nature of the channel, Monte Carlo simulations must be performed to obtain a reliable result from the channel model.

4.1.2. Simulation Scenario

A heterogeneous set of propagation scenarios was chosen for simulations, as shown in Table 1. For all these scenarios, Monte Carlo simulations were performed with 10,000 realisations, where the position of the transmit antenna (primary user) was fixed at the origin and the receive antenna was randomly located in a $500\text{ m} \times 500\text{ m}$ area. The height of the transmitter for the indoor and micro-cell channels was 2 m while for the macro-cell, it was 32 m. The height of the sense node was always 1.5 m. The channel parameters were calculated for a frequency of 2.4 GHz.

Table 1. Winner II SCME channel scenarios.

Scenario	Definition	LOS/NLOS
A2	Indoor to outdoor	NLOS
B1	Typical urban micro-cell	LOS/NLOS
C1	Suburban	LOS/NLOS
C2	Typical urban macro-cell	NLOS
D1	Rural macro-cell	LOS/NLOS

At every sense location, the complex patterns of the antenna array were embedded into the complex power angular profile of the channel. The dissimilarity among the power received through directional patterns was computed through dissimilar directional opportunity analysis as shown in Figure 10. The threshold was chosen certain decibels below the maximum among directions, for every snapshot, as compared to the global maximum over all snapshots and directions in the proof-of-principle measurement campaign.

4.2. Directional Opportunity Analysis

4.2.1. Measured Antenna System

The performance of the measured sector antenna shown in Figure 8 was analysed first by embedding the azimuth patterns into the scenarios in Table 1. The power angular profile for D1 NLOS scenario for three consecutive simulation runs is shown in Figure 16. As a representative example, the power received by the three sectors at 2.4 GHz, for 100 realisations in scenario D1 NLOS is shown in Figure 17. It can be observed that the received power from different sectors of the measured antenna differs by 10 to 20 dB. This indicates the presence of directional opportunity for the measured antenna in rural scenario for a threshold level 10 to 20 dB below the maximum signal level. The opportunity and dissimilarity for this particular scenario for a threshold that is 20 dB below maximum per snapshot are shown in Figure 18. It can be observed that for the best case, about 50% directional opportunity exists for this antenna in a rural scenario.

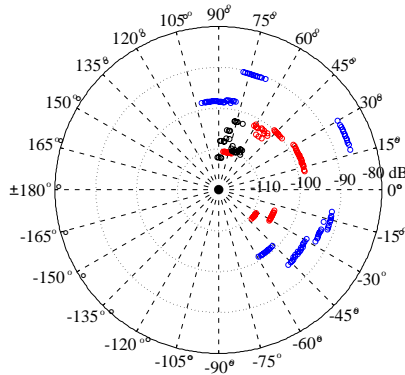


Figure 16. Power azimuth profile for scenario D1 NLOS at three random sense antenna locations shown by blue, red, and black colour respectively.

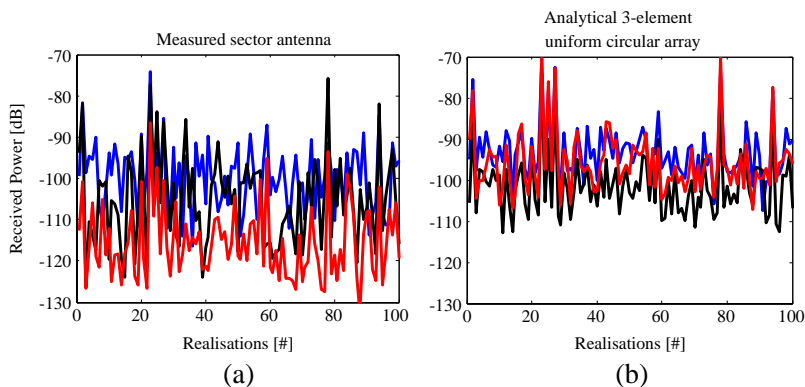


Figure 17. The power received at the first 100 snapshots by (a) the sector antenna shown in Figure 8 at 2.4 GHz and (b) a 3-element uniform circular array in scenario D1 NLOS. Different colours indicate the power received by different patterns.

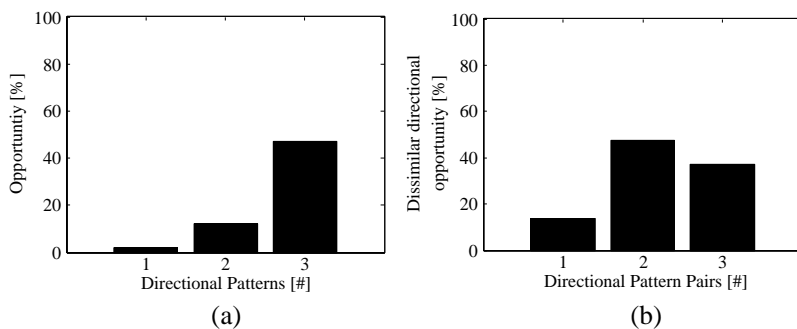


Figure 18. Opportunity seen by (a) measured sector antenna and dissimilarity among pairs d_1-d_2 , d_1-d_3 , and d_2-d_3 respectively for WINNER II scenario D1 NLOS and (b) a threshold that is 20 dB below maximum per snapshot.

In general, directional opportunities were seen for the measured patterns for all the scenarios under discussion. However, the measured sector antenna has narrow beamwidth and low sidelobe level due to the presence of metal walls between the array elements. Since such metal walls are not practical and would not exist in the antennas described in Section 2, it is reasonable to analyse various circular antenna arrays in these scenarios. To accomplish this analysis, analytical patterns of a circular array with an inter-element spacing of $\lambda/2$ were used.

4.2.2. Analytical Circular Array

Circular arrays of monopoles were analysed in the desired set of scenarios. The radiation patterns of these arrays were calculated from that of a dipole array with an addition of 3 dB in the gain. The radiation pattern of a dipole array can be computed from the element factor (EF) [29]

$$EF(\theta, \phi) = \eta \frac{|I_0|^2}{8\pi^2} \sin^3 \theta, \quad (1)$$

and the array factor (AF)

$$AF(\theta, \phi) = \sum_{n=1}^N I_n e^{jka[\sin \theta \cos(\phi - \phi_n) - \sin \theta_o \cos(\phi_o - \phi_n)]}, \quad (2)$$

as

$$\text{Array Pattern} = EF \times AF, \quad (3)$$

where θ and ϕ are the elevation and azimuth angles respectively, θ_o and ϕ_o are the desired beam direction, η is the free space impedance, I_0 is the current fed at the element port, k is the wave number, a is the radius of the circular array, I_n is the excitation coefficient, $\phi_n = \frac{2\pi}{N}$ and N is the number of elements in the array.

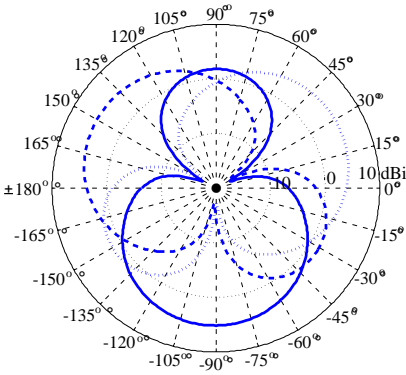


Figure 19. Analytical patterns of a 3-element uniform circular array used for comparison of a $\lambda/2$ array with the fabricated array in Figure 9. The patterns of the circular array are rotated and aligned to the measured patterns to obtain three sectors.

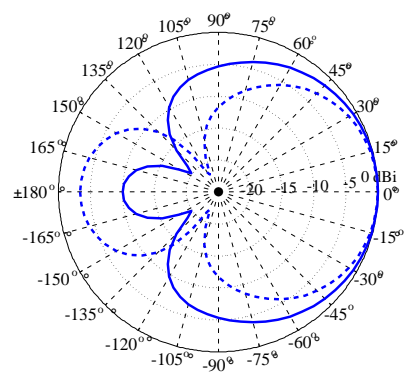


Figure 20. Analytical radiation patterns of a 3-element array with (solid) and without (dashed) sidelobe suppression (SLS).

When the radiation patterns of a uniform circular array of monopoles shown in Figure 19 were embedded into the complex power angular profiles for the scenario D1 NLOS, the resultant received power for 100 realisations as shown in the right-hand part of Figure 17 was obtained. It is clear that the analytical patterns receive more power than the measured patterns due to higher beamwidth and back-lobe level. Moreover, due to higher back-lobes, the received power levels from all three sectors are comparable, and hence result in less directional opportunity. However, side-lobe suppression algorithms can be applied to reduce the side-lobe level for this circular array.

4.3. Influence of Side-lobe Level of the Sense Antenna on Directional Opportunity

From basic antenna theory it is known that the side-lobe level of an antenna array can be reduced by tapering the amplitude of the excitation vectors of an array, where the narrowest beam is achieved with uniform excitation but at the expense of the highest side-lobe level. For the simulations described below, the side-lobe level was suppressed by applying a Chebyshev window to the phase-mode excitation vectors of the circular array, as described in [30]. The effect of side-lobe suppression for a 3-element array can be seen in Figure 20. It can be seen that the beamwidth of the antenna becomes wide as the side-lobes are suppressed through windowing. It should be further noticed that a very narrow beam with very low side-lobe level cannot be created using a small number of weakly directive elements. The side-lobe level of the array pattern can be reduced further by adding more elements in the array.

Directional opportunity for a 3-element uniform circular array is compared with the circular array with side-lobe suppression in Figure 21. Dissimilar directional opportunity was calculated for the arrays considering different threshold levels. It was observed that by reducing the side-lobe level, the percentage dissimilarity increased by about 20% especially for the non-line-of-sight (NLOS) scenarios, showing a similar trend for all propagation scenarios. It can be concluded from Figure 21 that the optimum threshold level is proportional to the side-lobe level of the radiation patterns. The array with suppressed side-lobes shows significant directional opportunity at 10 dB threshold while much less directional opportunity is observed for uniform circular array. Hence, the side-lobe level plays a key role in defining directional opportunities by influencing the threshold level. The rural scenario shows similar opportunity level for LOS and NLOS cases, possibly because of the inherent directional nature of multipath.

4.4. Influence of Array Size on Directional Opportunity

As seen in Figure 21, directional opportunity drastically drops beyond a threshold of 10 dB. Side-lobe level was identified as the most important contributor to the directional opportunity. Limited suppression was achievable for three elements, therefore, the effect of the number of elements on directional opportunity is studied in this section.

The number of elements considered for this study were 3 to 12 elements in a circular arrangement with inter-element spacing of $\lambda/2$. Patterns with side-lobe suppression were considered, while the side-lobe levels were suppressed to the minimum level possible with the indicated number of elements. As seen in Figure 22, the monopole antennas cannot provide very low side-lobe levels while employing a very small number of elements in an array.

Figure 23 shows the directional opportunity on an average as the patterns were rotated over the whole azimuth with N ($=$ number of elements) angular steps. It is apparent from this plot that a saturation is achieved for 6 elements, where directional opportunity ranging from 20 to 50% was observed for all scenarios. Beyond this, increasing the number of elements does not increase the average directional opportunity. The decrease in directional opportunity for scenario A2 can be attributed to the directional nature of multipath. Moreover, the beamwidth becomes narrower as the number of elements is increased

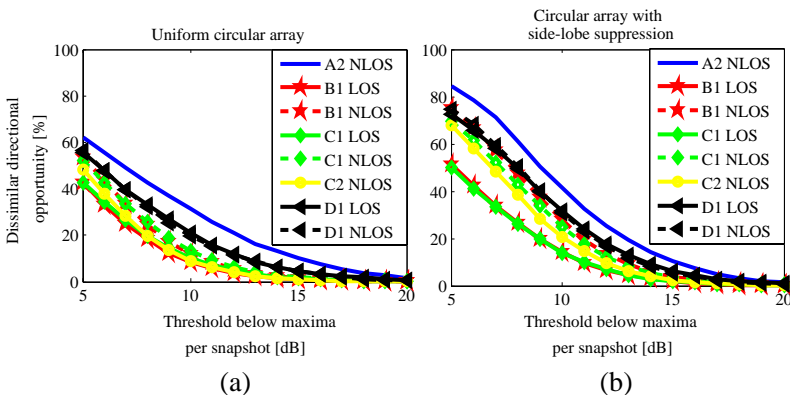


Figure 21. Percentage dissimilarity among patterns of a 3-element array versus threshold below instantaneous maximum for (a) uniform excitation and (b) side-lobe suppression. The results are shown for LOS (solid) and NLOS (dashed) scenarios detailed in the legend (c.f., Table 1).

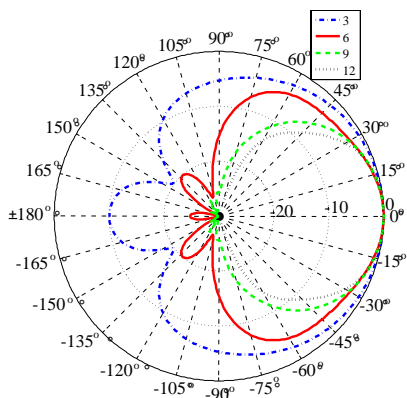


Figure 22. Analytical radiation patterns of a 3-, 6-, 9-, and 12-element circular array with maximum achievable side-lobe suppression (SLS).

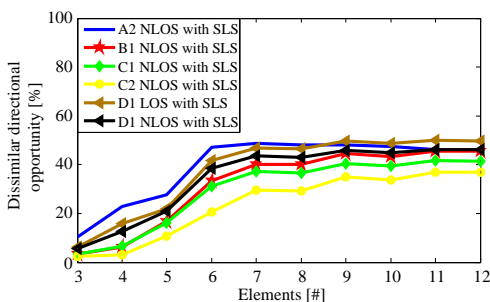


Figure 23. Dissimilar directional opportunity versus number of elements for a threshold that is 15 dB below instantaneous maximum per snapshot. The values shown are the mean of the opportunities for the patterns rotated over the whole azimuth.

as shown in Figure 22. This decrease in beamwidth also plays a role in the selection of the optimal antenna for directional communication in CR. The opportunity was observed to decrease as the angular spread of the channel becomes lower than the beamwidth of the antenna array, for example, for scenario A2 in Figure 23. Similarly for rural LOS scenario, a strong LOS component was observable, giving rise to an increased opportunity compared with NLOS case.

Based on this analysis, it may be concluded that a 6-element array with side-lobe suppression provides maximum directional opportunity in multipath scenarios for a reasonable level of threshold. The influence of threshold level on a 6-element array is shown in Figure 24, where

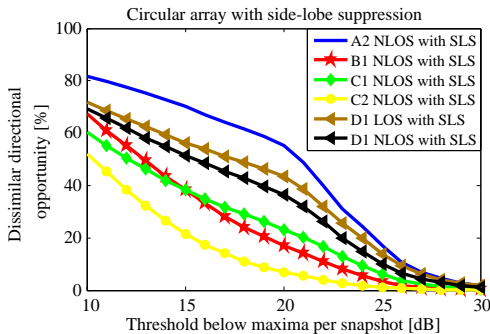


Figure 24. Dissimilar directional opportunity among patterns of a 6-element array versus threshold below instantaneous maximum for sidelobe suppression.

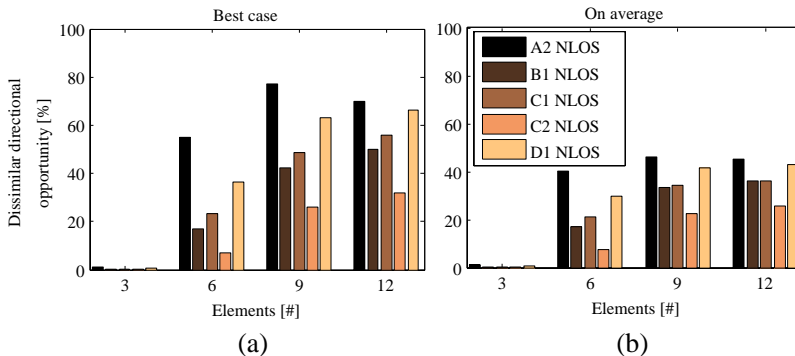


Figure 25. Dissimilar opportunity versus number of elements for a threshold that is 20 dB below instantaneous maximum per snapshot, for (a) the patterns pointing at opposite directions and (b) on average when the patterns were rotated over the whole azimuth. The results are shown for the case of side-lobe suppression (SLS) only.

reasonable directional opportunity is observed at a threshold of 20 dB.

The percentage dissimilar directional opportunity for the best case, when the patterns are pointing in opposite directions, and on average when the patterns are rotated over azimuth, are shown in Figure 25. It can be seen here that for a threshold level 20 dB below the instantaneous maximum per snapshot, saturation is achieved for 9 elements. However, 9-element-arrays may not be worth the incremental improvement given a significant increase of complexity compared with 6-element array, especially if we consider the average

over whole azimuth.

From these simulations, it is concluded that the antenna for directional CR communication should have low side-lobe level and narrow beamwidth, where the effect of the side-lobe level is dominant. The optimum side-lobe level depends on the chosen threshold, while a side-lobe level of 20 dB is found to be reasonable. A 6-element monopole array is capable of providing desired side-lobe level and, hence, sufficient directional opportunity at a threshold level of 20 dB. Other types of antenna arrays (patch, slot et cetera) may produce different results, pertaining to their element patterns and geometry. Furthermore, since the chosen spatial channel model provides power angular profiles in a stochastic way, the conclusions from these simulations can be generalised for any spatial channel model.

5. CONCLUSIONS

Multi-band directional antennas with spectral and directional selectivity are proposed to extend the parameter space for cognitive radio. The design concept of an appropriate compact multi-band antenna system is presented. The feasibility of such antennas for identification of frequency and directional resources is verified by line-of-sight measurements of a laboratory version of the proposed antenna in an over-the-air test setup. The existence of directional resources for cognitive radio in a multipath scenario is verified through an outdoor measurement campaign using the laboratory version of the proposed antenna. Simulations are then performed to test various kinds of antennas in heterogeneous propagation scenarios. The simulation results indicate that the side-lobe level of the antenna, dictated by the number and geometrical arrangement of elements in the array, influence the performance of directional sensing. A side-lobe level of 20 dB is suggested for the antenna design for directional cognitive radio communication. The 6-element circular array of monopoles provides 5 to 60% directional opportunity for heterogeneous propagation scenarios at the recommended threshold level of 20 dB. The use of a 6-element half-wavelength array would, however, be impractical for mobile platforms. Hence, an electrically small array with a suitable feed network, possibly reconfigurable, is suggested to cater with the effect of mutual coupling, and to define simultaneously accessible directional patterns. Moreover, digital beamforming can open up additional degrees-of-freedom on receive (for example, estimation of direction-of-arrival) and transmit (for example, optimal array operation).

The paper presents a preliminary analysis for identification of

directional opportunities. To assist the work of the proposed antenna system, each degree-of-freedom can be dealt with separately using the existing spectrum sensing algorithms, and the directional opportunity analysis can be performed at the end as described in this paper. The conventional spectrum sensing algorithms may also be extended to sophisticated directional spectrum sensing algorithms to deal with frequency and directional resources simultaneously.

ACKNOWLEDGMENT

This work has been funded by the the German Research Foundation (DFG) in the framework of the International Graduate School on Mobile Communications (MobiCom-GRK 1487) at Ilmenau University of Technology, Germany. The authors would like to thank M. Grimm, A. Krah, C. Schneider and W. Kotterman from Institute for Information Technology, Ilmenau University of Technology, and A. Heuberger from Fraunhofer IIS for their contributions in the proof-of-principle measurements and discussions.

REFERENCES

1. Federal Communications Commission, Spectrum Policy Task Force Report, ET Docket No. 02-135, Nov. 2002.
2. Wellens, M., J. Wu, and P. Mähönen, "Evaluation of spectrum occupancy in indoor and outdoor scenario in the context of cognitive radio," *Proc. 2nd Intl. Conf. on Cognitive Radio Oriented Wireless Networks and Commun.*, 420–427, Aug. 2007.
3. Mitola, III, J. and G. Q. Maguire, Jr., "Cognitive radio: Making software radios more personal," *IEEE Pers. Commun.*, Vol. 6, No. 4, 13–18, Aug. 1999.
4. Haykin, S., "Cognitive radio: Brain-empowered wireless communications," *IEEE J. Sel. Areas in Commun.*, Vol. 23, No. 2, 201–220, Feb. 2005.
5. Sharma, R. K. and J. W. Wallace, "Correlation-based sensing for cognitive radio networks: Bounds and experimental assessment," *IEEE Sensors J.*, Vol. 11, No. 3, 657–666, Mar. 2011.
6. Urkowitz, H., "Energy detection of unknown deterministic signals," *Proc. IEEE*, Vol. 55, No. 4, 523–531, Apr. 1967.
7. Yucek, T. and H. Arslan, "A survey of spectrum sensing algorithms for cognitive radio applications," *IEEE Communications Surveys and Tutorials*, Vol. 11, No. 1, 116–130, First Quarter 2009.

8. Hall, P. S., P. Gardner, and J. Kelly, "Reconfigurable antenna challenges for future radio systems," *Proc. 3rd Intl. Conf. on Antennas and Propag.*, 949–955, Mar. 2009.
9. Ghanem, F., P. S. Hall, and J. R. Kelly, "Two port frequency reconfigurable antenna for cognitive radios," *Electronics Letters*, Vol. 45, No. 11, 534–536, May 21, 2009.
10. Tawk, Y., J. Costantine, and C. G. Christodoulou, "A rotatable reconfigurable antenna for cognitive radio applications," *IEEE Radio and Wireless Symposium (RWS)*, 158–161, Jan. 16–19, 2011.
11. Al-Husseini, M., A. El-Hajj, Y. Tawk, K. Y. Kabalan, and C. G. Christodoulou, "A simple dual-port antenna system for cognitive radio applications," *2010 International Conference on High Performance Computing and Simulation (HPCS)*, 549–552, Jun. 28–Jul. 2, 2010.
12. Hamid, M. R., P. Gardner, P. S. Hall, and F. Ghanem, "Switched-band vivaldi antenna," *IEEE Trans. Antennas Propag.*, Vol. 59, No. 5, 1472–1480, May 2011.
13. Zamudio, M. E., Y. Tawk, J. Costantine, S. E. Barbin, and C. G. Christodoulou, "Reconfigurable filter embedded into an antenna for UWB cognitive radio environment," *Proc. IEEE — APS Topical Conf. on Antennas and Propag. in Wireless Commun.*, 714–717, Sep. 2011.
14. Reed, J. H., J. T. Bernhard, and J. Park, "Spectrum access technologies: The Past, the present, and the future," *Proc. IEEE*, Vol. 100, 1676–1684, May 2012.
15. Nishimori, K., R. D. Taranto, H. Yomo, P. Popovski, Y. Takatori, R. Prasad, and S. Kubota, "Spatial opportunity for cognitive radio systems with heterogeneous path loss conditions," *Proc. Vehicular Techn. Conf.*, 2631–2635, Apr. 2007.
16. Zhao, G., J. Ma, G. Y. Li, T. Wu, Y. Kwon, A. Soong, and C. Yang, "Spatial spectrum holes for cognitive radio with relay-assisted directional transmission," *IEEE Trans. Wireless Commun.*, Vol. 8, No. 10, 5270–5279, Oct. 2009.
17. Taranto, R. D., K. Nishimori, P. Popovski, H. Yomo, Y. Takatori, R. Prasad, and S. Kubota, "Simple antenna pattern switching and interference-induced multi-hop transmissions for cognitive radio networks," *Proc. IEEE 2nd Intl. Symposium on New Frontiers in Dynamic Spectrum Access Networks*, 543–546, Apr. 2007.
18. Mirkimali, A. and P. S. Hall, "Log periodic printed dipole array for wideband frequency reconfiguration," *IET Seminar on Wideband, Multiband Antennas and Arrays for Civil or Defence Applications*,

- 95–110, Mar. 2008.
19. Freeman, J. L., B. J. Lamberty, and G. S. Andrews, “Optoelectronically reconfigurable monopole antenna,” *Electronics Letters*, Vol. 28, No. 16, 1502–1503, Jul. 1992.
 20. Nikolaou, S., R. Bairavasubramanian, C. J. Lugo, I. Carrasquillo, D. C. Thompson, G. E. Ponchak, J. Papapolymerou, and M. M. Tentzeris, “Pattern and frequency reconfigurable annular slot antenna using PIN diodes,” *IEEE Trans. Antennas Propag.*, Vol. 54, No. 2, 439–448, Feb. 2006.
 21. Kraus, A., M. Grimm, N. Murtaza, W. Kotterman, M. Landmann, A. Heuberger, R. Thom, and M. Hein, “Over-the-air test strategy and testbed for cognitive radio nodes,” *2011 XXXth URSI General Assembly and Scientific Symposium*, 1–4, Aug. 13–20, 2011.
 22. Murtaza, N., M. A. Hein, and E. Zameshaeva, “Reconfigurable decoupling and matching network for a cognitive antenna,” *Proc. of European Microwave Conference*, 874–877, Oct. 2011.
 23. Yong, C. and Y. J. Guo, “A frequency-agile compact array with a reconfigurable decoupling and matching network,” *IEEE Antennas and Wireless Propagation Letters*, Vol. 10, 1031–1034, 2011.
 24. Murtaza, N., A. Kraus, M. Grimm, A. Heuberger, R. Thoma, and M. Hein, “Multi-band direction-sensitive cognitive radio node,” *Proc. IEEE — APS Topical Conf. on Antennas and Propag. in Wireless Commun.*, 251–254, Sep. 2011.
 25. Ettus Research, Online Available: <http://www.ettus.com>.
 26. Tandur, D., J. Duplicy, K. Arshad, D. Depierre, K. Moessner, J. Lehtomaki, K. Briggs, L. Goncalves, and A. Gameiro, “Cognitive radio systems evaluation: measurement, modeling, and emulation approach,” *IEEE Vehicular Technology Magazine*, Vol. 7, No. 2, 77–84, Jun. 2012.
 27. Vodafone D2, Online Available: <http://www.vodafone.de>.
 28. Winner II Spatial Channel Model, Online Available: <http://www.ist-winner.org/phase-2-model.html>.
 29. Balanis, C. A., *Antenna Theory: Analysis and Design*, 3rd Edition, Wiley-Interscience, May 2005.
 30. Belfiori, F., S. Monni, W. V. Rossum, and P. Hoogeboom, “Side-lobe suppression techniques for a uniform circular array,” *Proc. 7th European Radar Conf.*, 113–116, Sep. 2010.